

Femto-Satellite Clusters Decentralized Control Strategy Based on Aerodynamic Forces

Fatima Alnaqbi¹ and Shamil Bikitimirov¹

¹Propulsion and space research center, Technology Innovation institute, United Arab Emirates (UAE),
e-mails: fatima.alnaqbi@tii.ae, bikitimirovshamil@gmail.com

ABSTRACT

FemtoSats can be highly considered for cluster missions due to their relatively low mass (< 100 g), small size, and low cost compared to other types of satellites. One of the main challenges with FemtoSats is their limited capabilities to be equipped with thrusters for relative motion control. To overcome this problem, we propose to use a decentralized differential aerodynamic force-based control algorithm to maintain the required cluster configuration. In order to keep the cluster bounded, the along-track drift caused by the difference in the satellite's orbit periods should be eliminated. On the other side, the instantaneous ellipse's center shift and ellipse size of the relative motion trajectory should be within the boundaries to satisfy the requirements on the inter-satellite communication distance. All three parameters must be controlled using only atmospheric drag force which imposes constraints on both the magnitude and direction of the control input. Lyapunov function-based (LF) control derived based on Gauss Variation Equations is used to keep track of relative motion geometrical parameters using differences in orbital elements. The control gains were tuned via Monte Carlo simulations for decentralized control of a swarm of two satellite. A novel decentralized satellite cluster control approach is presented and a set of rules were used to define the control input for each satellite within the cluster. A comprehensive numerical simulation of the satellite cluster dynamics and control is performed to demonstrate the efficiency of the proposed satellite cluster control algorithms for different initial conditions. The numerical study demonstrates that the proposed decentralized control approach effectively controls the relative motion between a swarm of FemtoSats, relying solely on atmospheric drag force.

I. Introduction

Distributed satellite systems have gained a lot of attention as they introduce several advantages over conventional single satellite missions. Satellite cluster is one type of distributed system where satellites are placed intentionally close to each other and they work together to achieve

one common goal. The size and the number of satellites in the cluster can vary based on the mission requirements and application. Hundreds to thousands of satellites might be needed to achieve the required objective and to have real-time distributed measurements or sensing for a specific science goal.

FemtoSats impose different advantages over other larger satellites in terms of cost, mass, and size. The size of the FemtoSats can be in the range of 0.01–0.1 m with a mass of less than 100 g and cost around \$100–20,000 [1; 2]. As a result, a large number of FemtoSats can be deployed to meet the required needs at a relatively low cost. A number of research groups are investigating and developing FemtoSats platforms for different types of applications. Different applications were found in literature including large-area space phenomena and space weather monitoring, measuring magnetic field variation around a planet or a spacecraft, and asteroid mapping missions.

Teale et al. [3] investigated the possibility of using massively distributed in-situ parallel sensing (MDIPS) to study the unmodelled Earth magnetospheric events. Their study shows an improvement in the sampling rate compared to a single satellite or a small-size cluster system. For some specific missions, the state of the Earth's magnetic field in LEO should be monitored within a very short duration (< 1 hour). Therefore, the reduced revisit time achieved by MDIPS will give a much faster monitoring rate for the magnetic field.

Hadaegh et al. [4] proposed a novel swarm of silicon wafer-integrated FemtoSats (SWIFT) to be used for potential sparse aperture arrays and distributed sensor networks. They presented different Golay swarm configurations using different numbers of FemtoSats (200 - 1200 FemtoSats). The Golay-12 configuration showed the largest effective access diameter compared to other configurations with a fixed number of FemtoSats. This allows significantly to have a wider range of ground access with reduced system mass and cost.

However, the biggest challenge with FemtoSats is the lack of volume and mass which makes it difficult to integrate the major satellite components and subsystems in a very small board or chip. For instance, constraints in mass

and size limit the communication range of FemtoSats due to restrictions on transmission power. Because of that, decentralized inter-satellite communication is needed to overcome this problem. On the other hand, the limitation of the FemtoSats restricts the possibility of adding active actuators i.e. thrusters and reaction wheels for position and attitude control. Therefore, FemtoSats are usually launched as free-flying spacecrafts thus causing a cluster decomposition due to the uncontrolled relative drift between satellites which makes the mission lifetime very short. Hadaegh et al. [4] pointed out the importance of controlling the relative position of the satellite within the cluster to keep the motion bounded and to get the required configuration. They proposed several candidate propulsion systems i.e. electrospray thrusters to be used for FemtoSats which weigh less than 40 g and provide thrust up to 100 μ N [4]. However, the limited fuel will restrict the duration of control, leading to a short mission lifetime due to the uncontrolled drifting motion and relative trajectories

To eliminate this problem, passive control techniques i.e. aerodynamic force and Lorentz forces can be considered for relative position control. Different control algorithms were discussed in the literature for relative motion control such as linear-quadratic regulators (LQR), Lyapunov-based control (LF), and Artificial potential function (APF). D. Ivanov et al. [5] discussed the centralized and decentralized control approaches using LQR and LF for a swarm of 3U CubeSats. It shows the implementation of both control algorithms to maintain the required swarm configuration. The main objective was to eliminate the relative drift and along-track shift between the CubeSats caused by the difference in CubeSats deployment velocity. Overall, the proposed control algorithms were able to successfully converge to the required swarm structure taking into account the limitation on differential drag control force.

In another paper, D. Ivanov et al. [6] conducted a detailed analysis of the motion of 3U CubeSats swarm under varying initial deployment velocity errors, considering constraints imposed by communication range and the aerodynamic control force. The proposed decentralized LF-based control and control rules provide the required swarm distribution in an along-track direction. Hill-Clohessy-Wiltshire (HCW) equations constants c_1 and c_4 are considered to eliminate the relative motion drift and shift. Collision avoidance among swarm agents was also considered. A control force is applied if a CubeSat enters the collision risk area of another CubeSat, helping to prevent potential collisions. This results in a deviation of the relative motion ellipses' centers, but finally, the control was able to settle down the centers' shift to up to 500 m. On the other hand, higher error in the deployment velocity can cause the swarm to split into several independent groups due to the limitation in the communication sphere of each CubeSat. Further study was proposed to address this issue.

The paper has the following structure. Section II. describes the problem statement of this study. In section III., the dynamic equations of the orbital motion are discussed including the considered aerodynamic acceleration equations that are used for control. Section IV. illustrates the relative motion geometry using HCW equations constants and differences in orbital elements. Section V. describes the LF-based control algorithm and its implementation in the problem. For a swarm of FemtoSats, decentralized control approach is developed and presented in section VI.. The simulation and results are shown in section VII.. Finally, the discussion and conclusion are presented in section VIII..

II. Problem Statement

Satellite cluster requires an advanced control algorithm to track precisely the relative motion between satellites and drive them to the required position to form the needed cluster configuration. However, FemtoSats can be hardly equipped with thrusters to provide the required control force due to their limited mass and geometry. Therefore, in this study, we propose to use the drag force in low Earth orbits to control the relative position of the FemtoSats within the cluster. To achieve maximum differential aerodynamic force, we consider FemtoSats that have the dimensions of a Printed Circuit Board satellite (PCBSat) with a high ballistic coefficient such that the thickness of the satellite is much smaller than the length and the width. Magnetorquers are considered for the attitude control to switch between attitudes yielding the required drag force to control satellite relative motion. Since the lift force is very small compared to the drag force, we consider the lift force as one of the disturbances to the system. It should be noted that the aerodynamic force-based control utilization imposes constraints on the control force direction and magnitude due to the high ratio between drag and lift forces that can be used to control the relative motion between FemtoSats within the cluster. As a result, certain control approaches such as the artificial potential function-based (APF) method may not be suitable for this application, as they might necessitate control forces that cannot be implemented using aerodynamic forces alone.

In previous study [7], the relative motion of FemtoSats was controlled using LF based on HCW equations' constants, c_1 and c_4 . Decentralized aerodynamic force-based control was applied to converge to the required relative distances between all swarm particles and to eliminate the drift caused by c_1 . The study took into account the limitation on charging and power capacity. It proposes a number of rules to determine for each satellite an instantaneous set of surrounding satellites that are taken into account when computing the relative control input. Following the rules and limitations, the derived control law was able to satisfy the objectives of the study. However, using LF based on c_1 and c_4 only does not allow us to control the size of the relative trajectories. Therefore,

we propose to use LF based on difference in orbital elements $\delta\epsilon$ instead of HCW constants. This should give more insights about the control parameters and provide better control for each specific orbital element.

III. Equations of motion

The satellite orbital motion dynamics used in this paper is described by Eq. 1 written in the ECI frame $OXYZ$ denoted as \mathcal{F}^I (see Fig. 1). Accelerations due to the Earth oblateness \mathbf{a}_{J_2} and aerodynamic force \mathbf{a}_{aero} are considered. The satellite state vector given in \mathcal{F}^I is denoted by $\mathbf{X} = [\mathbf{R}^T, \mathbf{V}^T]^T$.

$$\ddot{\mathbf{R}} = -\frac{\mu\mathbf{R}}{R^3} + \mathbf{a}_{aero} + \mathbf{a}_{J_2}, \quad (1)$$

$$\mathbf{a}_{J_2} = \frac{3\mu J_2 \mathcal{R}_\oplus^2}{2R^5} \left[\left(\frac{5Z^2}{R^2} - 1 \right) \mathbf{R} - 2\mathbf{Z} \right],$$

where $\mathbf{Z} = [0, 0, Z]^T$.

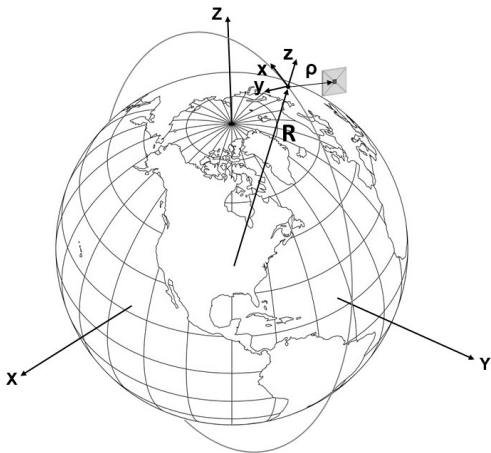


Figure 1: Reference frames.

In this paper, the aerodynamic force model proposed by [8] is considered for the numerical study and simulations. It takes into account the drag and lift forces acting on a flat plate which corresponds to the considered PCBsat in this paper.

The attitude of the PCBsat determines the acceleration due to the aerodynamic force. Changing the direction of the PCBsat normal vector n (see Fig. 2) varies the magnitude of the drag and lift forces. The direction of n is defined by the two angles θ and ϕ as shown in the figure. The acceleration vector \mathbf{a}_{aero} can be written as function of θ and ϕ :

$$\mathbf{a}_{aero} = k \begin{bmatrix} p(\theta) \\ g(\theta) \cos \phi \\ g(\theta) \sin \phi \end{bmatrix} \quad (2)$$

where $k = \frac{1}{2}\rho v_{rel}^2 A/m$, ρ is the atmospheric density, $v_{rel} = |\mathbf{V} - \boldsymbol{\omega}_\oplus \times \mathbf{R}|$ is the velocity relative to the atmosphere, $\boldsymbol{\omega}_\oplus$ is the Earth angular velocity vector given in \mathcal{F}^I , A is the satellite's surface area, and m is the satellite's mass.

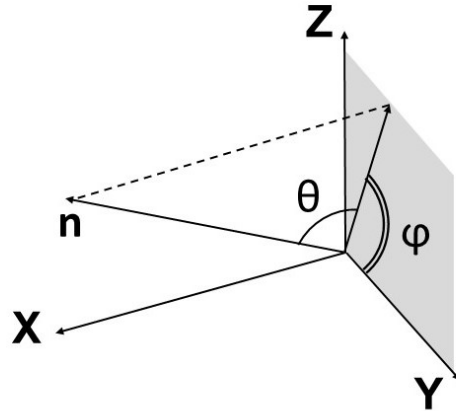


Figure 2: PCBsat attitude angles.

$p(\theta)$ and $g(\theta)$ are both functions of angle of attack θ where they describe the drag force and lift force components respectively:

$$\begin{aligned} p(\theta_i) &= -2\varepsilon(\sin \theta_i)^3 + \eta(\varepsilon - 1)(\sin \theta)^2 + \\ &\quad (\varepsilon - 1) \sin \theta_i, \\ g(\theta_i) &= -\cos \theta_i \sin \theta_i (\eta - \eta\varepsilon + 2\varepsilon \sin \theta_i) \end{aligned} \quad (3)$$

In the context of aerodynamic forces, it's noted that the lift force's magnitude is significantly smaller than that of the drag force component. Consequently, the control of relative motion between satellites relies solely on the drag force, while the lift force component is eliminated. This simplifies the control approach, focusing exclusively on the more dominant drag force to effectively control satellite motion.

IV. Relative motion geometry

For satellite relative motion control, the linearized equations of motion, the Hill-Clohessy-Wiltshire (HCW) equations [9; 10] and its analytical solution are considered. The equations are derived with respect to the orbital frame \mathcal{F}^O (see Fig. 1), where z -axis is aligned with the local vertical, y -axis is along the angular momentum vector of the target orbit, and x -axis completes the right-handed orthogonal coordinate frame. Satellite's state vector given in \mathcal{F}^O is denoted by $\mathbf{x}_i = [\boldsymbol{\rho}_i^T, \mathbf{v}_i^T]^T$. The HCW equations are given by:

$$\begin{cases} \ddot{x} + 2n\dot{z} = 0, \\ \ddot{y} + n^2y = 0, \\ \ddot{z} - 2n\dot{x} - 3n^2z = 0. \end{cases} \quad (4)$$

where n is the mean motion for the target orbit.

The analytical solution to the HCW equations can be written in the amplitude-phase form as

$$\begin{cases} x(t) = 3c_1nt + \rho_1 \cos(nt + \alpha_1) + c_4, \\ y(t) = \rho_2 \sin(nt + \alpha_2), \\ z(t) = -2c_1 + \frac{\rho_1}{2} \sin(nt + \alpha_1). \end{cases} \quad (5)$$

where $\rho_1 = 2\sqrt{c_2^2 + c_3^2}$, $\alpha_1 = \tan^{-1}(\frac{c_3}{c_2})$, $\rho_2 = \sqrt{c_5^2 + c_6^2}$, $\alpha_2 = \tan^{-1}(\frac{c_6}{c_5})$ and constants $c_1 - c_6$ are as follows

$$\begin{cases} c_1 = -2z_0 - \dot{x}_0/n, \\ c_2 = \dot{z}_0/n, \\ c_3 = -3z_0 - 2\dot{x}_0/n, \\ c_4 = x_0 - 2\dot{z}_0/n, \\ c_5 = \dot{y}_0/n, \\ c_6 = y_0. \end{cases} \quad (6)$$

As can be noticed from Eq. 5, c_1 constant represents the along track drift of the satellite with respect to the target, whereas c_4 represents the along track separation. The relative trajectory ellipse's dimension is determined by ρ_1 and ρ_2 as shown in Fig. 3.

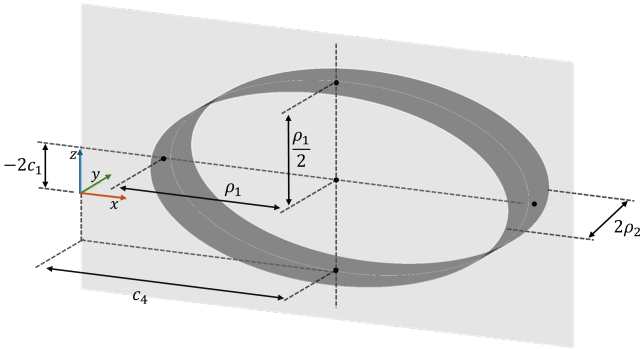


Figure 3: Instantaneous (no drift) relative motion trajectory representation using HCW constants.

A. Linear Mapping Between Hill Frame Coordinates and Orbit Element Differences

Another approach to write the relative state vector \mathbf{x}_i is to use difference in orbital elements $\delta\mathbf{\alpha}$ instead of HCW constants. The generalized linear mapping between orbital frame state vector and orbital element difference is described in [11]. The orbit element difference vector is defined as:

$$\delta\mathbf{\alpha} = \mathbf{\alpha}_d - \mathbf{\alpha}_c,$$

where $\mathbf{\alpha}_d$ and $\mathbf{\alpha}_c$ are the deputy and chief satellites orbital elements respectively and $\mathbf{\alpha} = [a, e, i, \Omega, \omega, M]^T$.

However, in order to compare this approach with HCW equations, the simplified mapping equations for a near circular chief orbit is considered which are also discussed in [11]. Setting the initial true anomaly of the chief satellite f_0 to zero, \mathbf{x}_i can be written in term of $\delta\mathbf{\alpha}$ as follows:

$$\begin{cases} x(t) = -2a \sin(f)\delta e + a(\delta\omega + \delta M \\ \quad + \cos(i)\delta\Omega) - \frac{3}{2}f\delta a, \\ y(t) = a\sqrt{\delta i^2 + \sin^2(i)\delta\Omega^2} \cos(\theta - \theta_z), \\ z(t) = a \cos(f)\delta e + \delta a. \end{cases} \quad (7)$$

where $f = nt$ is the chief true anomaly, θ is the chief argument of latitude and $\theta_z = \arctan(\frac{\delta i}{-\sin(i)\delta\Omega})$.

Using Eq. 5 and Eq. 7 the mapping between HCW equations constants and $\delta\mathbf{\alpha}$ can be written as follows (assuming $\delta\theta_0 = 0$ and $f_0 = 0$):

$$\begin{cases} c_1 = -\delta a/2, \\ \rho_1 = 2a\delta e, \\ \rho_2 = a\delta\gamma, \\ c_4 = a\delta\lambda - \rho_1 \sin(f) \\ \alpha_1 = 0, \\ \alpha_2 = -\theta_z. \end{cases} \quad (8)$$

where $\gamma = \sqrt{\delta i^2 + \sin^2(i)\delta\Omega^2}$ and $\delta\lambda = \delta\omega + \delta M + \cos(i)\delta\Omega$.

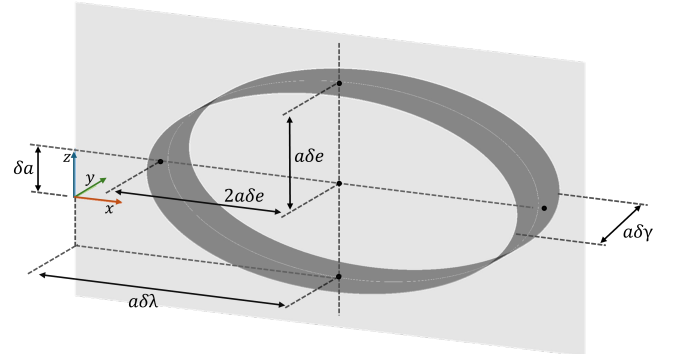


Figure 4: Instantaneous (no drift) relative motion trajectory representation using $\delta\mathbf{\alpha}$.

V. Lyapunov function based control

In this paper, a Lyapunov function feedback control law based on mean orbital elements difference is considered. The error in orbital elements $\delta\mathbf{\alpha}$ is defined as the difference between current deputy orbital elements $\mathbf{\alpha}_d$ and the desired deputy orbital elements $\mathbf{\alpha}_{dd}$:

$$\delta\mathbf{\alpha} = \mathbf{\alpha}_d - \mathbf{\alpha}_{dd},$$

$$\boldsymbol{\alpha}_{dd} = \boldsymbol{\alpha}_c + \Delta\boldsymbol{\alpha}$$

where $\Delta\boldsymbol{\alpha}$ is the fixed set of mean orbit element difference.

For the purpose of control, the mean orbit element rate equation is approximated as:

$$\dot{\boldsymbol{\alpha}} \approx [A(\boldsymbol{\alpha})] + [B(\boldsymbol{\alpha})]\mathbf{u} \quad (9)$$

where $[A(\boldsymbol{\alpha})]$ matrix describes the behaviour of the orbit elements under J_2 effect and control influence matrix $[B(\boldsymbol{\alpha})]$ is developed using Gauss' variational equations:

$$[A(\boldsymbol{\alpha})] = \begin{bmatrix} 0 \\ 0 \\ 0 \\ -\frac{3}{2}J_2\left(\frac{r_p q}{p}\right)^2 n \cos i \\ \frac{3}{4}J_2\left(\frac{r_p q}{p}\right)^2 n (5 \cos^2 i - 1) \\ n + \frac{3}{4}J_2\left(\frac{r_p q}{p}\right)^2 \eta n (3 \cos^2 i - 1) \end{bmatrix}$$

$$[B(\boldsymbol{\alpha})] = \begin{bmatrix} \frac{2a^2 e \sin f}{hr_e} & \frac{2a^2 p}{hrre} & 0 \\ \frac{p \sin f}{h} & \frac{(p+r) \cos f + re}{h} & 0 \\ 0 & 0 & \frac{r \cos \theta}{h} \\ 0 & 0 & \frac{r \sin \theta}{h \sin i} \\ -\frac{p \cos f}{he} & \frac{(p+r) \sin f}{he} & -\frac{r \sin \theta \cos i}{h \sin i} \\ \frac{\eta(p \cos f - 2re)}{he} & -\frac{\eta(p+r) \sin f}{he} & 0 \end{bmatrix}$$

A positive definite lyapunov control function based on mean orbit element tracking error $\delta\boldsymbol{\alpha}$ is used:

$$V(\delta\boldsymbol{\alpha}) = \frac{1}{2} \delta\boldsymbol{\alpha}^T \delta\boldsymbol{\alpha}. \quad (10)$$

Taking the derivative of V and substituting Eq.11, the control law is derived as follows (assuming the desired relative orbits is J_2 invariant where no control is required to maintain the orbit; $[B(\boldsymbol{\alpha}_{dd})]$ is neglected):

$$\mathbf{u} = -[B(\boldsymbol{\alpha}_d)]([A(\boldsymbol{\alpha}_d)] - [A(\boldsymbol{\alpha}_{dd})]) + [P]\delta\boldsymbol{\alpha}, \quad (11)$$

with $[P]$ being a positive definite feedback gain matrix which is a function of f and θ to make use of the fact that orbit elements are most controllable and least controllable at certain points in orbit.

A. Relative motion control example

To assess the effectiveness of the control law, a scenario involving two satellites is examined. In this scenario, one satellite is designated as the chief, while the other serves as the deputy. Centralized control is used for this example. Both satellites have the dimensions of PCBsat. The

initial orbital elements of the deputy satellite is defined by setting values for δa , $\delta \lambda$ and δe and sum it up with the corresponded initial chief orbital elements. The goal of the control law in this example is to eliminate $\delta\boldsymbol{\alpha}$ whereas $\Delta\boldsymbol{\alpha} = 0$. The deputy satellite relative trajectory should be finally bounded within the communication sphere of the chief satellite. Simulation parameters are summarized in Table 1. In this example, the control force was limited to $-e_\theta$ direction which represent the direction of the drag force, and the magnitude of the force was also limited to the atmospheric drag force magnitude at the given altitude.

Figure 5 shows the 3D trajectory of the deputy relative trajectory with respect to the chief satellite which is placed at origin in the figure. The control law was able to eliminate the drift and shift caused by δa and $\delta \lambda$ respectively. Also, the size of the relative ellipse trajectory was controlled and converged to a small value. The convergence of $\delta\boldsymbol{\alpha}$ is shown in Fig. 6. For comparison, HCW equations constants were calculated using Eq. 6 and plotted in Fig. 7. The plots visibly confirm the mapping illustrated in Eq. 8.

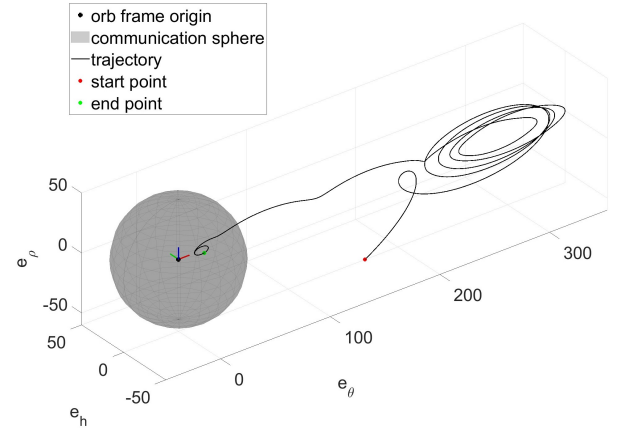


Figure 5: Two satellites centralized control trajectory.

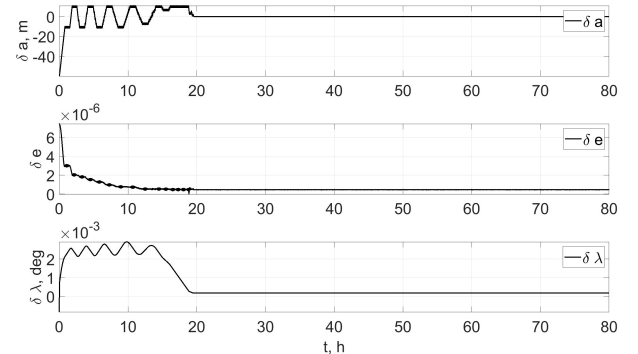


Figure 6: $\delta\boldsymbol{\alpha}$ variation for two satellites centralized control.

Table 1: Two satellites centralized control simulation parameters

Parameter	Value	Units
Satellite Parameters		
PCBSat mass, m	0.1	kg
PCB area, A	9×9.5	cm^2
Swarm parameters		
swarm population	2	-
δa_0	-60	m
$a\delta\lambda_0$	70	m
$a\delta e_0$	50	m
Control parameters		
communication sphere radius, r_{bound}	50	m
safe along track shift	30	m
max drift threshold	100	m

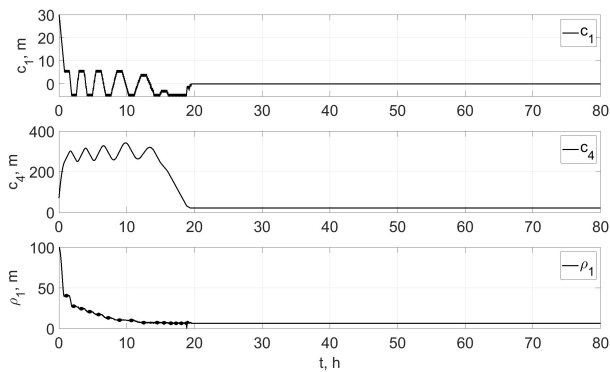


Figure 7: HCW constants variation for two satellites centralized control.

VI. Decentralized control approach

For a large swarm of FemtoSats, decentralized control is preferred over centralized control. This preference arises from the limitation that centralized reference information may not be available to all swarm agents due to communication constraints. Therefore, the following decentralized swarm control logic is proposed to converge to the required swarm configuration:

1. To calculate the control input for each satellite, all other satellites in the swarm are considered as peer satellites.
2. The inertial state vector \mathbf{X} and the relative state vector to the considered satellite \mathbf{x} are calculated.
3. The difference in orbital elements between each peer satellite and the considered satellite is calculated $\delta\mathbf{oe}$.
4. Two sets of rules are used to calculate the relative motion control input's component $u_x^i = -\sum_{j=1}^m u_x^j$ for an i -th satellite (the considered satellite):

- (a) The first set of rules are followed mainly to eliminate the drift and shift between the swarm

particles caused by δa and $\delta\lambda$ while also controlling the size of relative ellipse trajectory δe . The u_x^j is calculated for j -th satellite that satisfy the following rules:

- i. rule 1.1 - The satellite has a positive shift $\delta\lambda$ greater than the given threshold with respect to i -th satellite.
- ii. rule 1.2 - The satellite has either positive relative drift ($-\delta a$) or has a drift magnitude lower than a given threshold.

- (b) The second set of rules are used to control the size of the relative ellipse trajectory once δa and $\delta\lambda$ of j -th become less than the given threshold. In this case, a higher control gain is given to δe . The u_x^j is calculated for j -th satellite that satisfy the following rules:

- i. rule 2.1 - rule 1.1 and rule 1.2 both are not satisfied.
- ii. rule 2.2 - relative drift δa and relative shift $\delta\lambda$ are both less than the threshold.
- iii. rule 2.3 - relative ellipse size δe is more than the threshold.

5. Finally, u_x^i for the considered satellite is calculated by summing up all u_x^j calculated with respect to each peer satellite.

VII. Numerical study

A swarm of multiple satellites is considered for the decentralized control numerical study. The initial conditions for this simulation are presented in Table 2. The results are shown in Figs. 8, 9 and 10. It can be noticed that all swarm particles converged to the target and their final trajectories are bounded within the communication sphere using only atmospheric drag force.

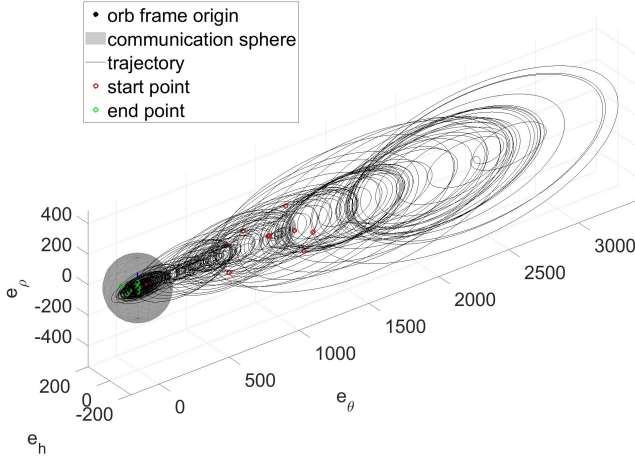


Figure 8: Decentralized control swarm trajectories.

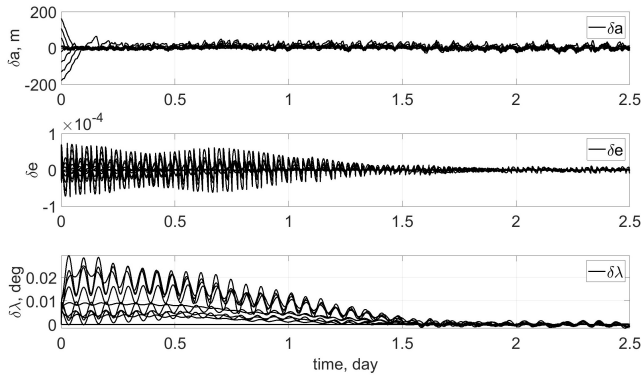


Figure 9: δoe constants variation for the swarm decentralized control.

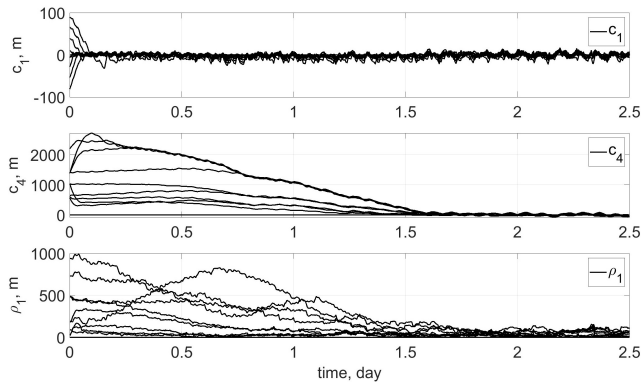


Figure 10: HCW constants variation for the swarm decentralized control.

VIII. Conclusion

This paper considered satellite swarm dynamics and control, utilizing aerodynamic forces. It introduces a novel decentralized swarm control algorithm, incorporating a set of rules to determine, for each satellite, an instantaneous set of peer satellites. These peers are considered when computing the relative control input, enhancing the overall swarm performance. Lyapunov function-based control was employed, utilizing the difference in orbital elements as the controlling variables. The effectiveness of the control algorithms is validated through numerical simulations of the orbital motion dynamics for a swarm of multiple satellite under control. The results indicate that the decentralized control approach successfully managed to control the relative motion trajectories of the swarm particles by effectively eliminating drift and shift. Furthermore, the size of the bounded relative trajectory was also successfully controlled which was not considered in previous papers.

Further investigation could explore achieving specific swarm configurations, such as concentric arrangements where the centers of relative ellipse trajectories coincide, while allowing for variations in the size of each ellipse. Furthermore, research could investigate the uniform distribution of swarm agents along the track direction to achieve specific goals. On the other hand, collision avoidance is crucial aspect in this type of missions where satellites operate close to each others. Hence, it's important to establish additional rules or control logic to prevent collisions among swarm particles.

References

- [1] "Small satellites: Technology that democratizes space." <https://eos.com/blog/small-satellites/>. Accessed: 2024-03-26.
- [2] D. J. Barnharta, T. Vladimirovaa, A. M. Bakerb, and M. N. Sweeting, "A low-cost femtosatellite to enable distributed space missions," *Acta Astronautica*, vol. 64, pp. 1123–1143, 2009.
- [3] C. Teale, J. Beeley, G. Bailet, and C. R. McInnes, "A novel femtosatellite sensor array for deconvolving time and space measurements of transient phenomenon in Earth orbit," *74th International Astronautical Congress (IAC)*, 2023.
- [4] F. Y. Hadaegh, S.-J. Chung, and H. M. Manohara, "On Development of 100-Gram-Class Spacecraft for Swarm Applications," *IEEE SYSTEMS JOURNAL*, 2014.
- [5] D. Ivanov, M. Ovchinnikov, and S. Tkachev, "Nanosatellites Formation Flying Control Approaches Overview," *IOP Conference Series: Materials Science and Engineering*, 2020.

Table 2: Satellite swarm decentralized control simulation parameters

Parameter	Value	Units
	Satellite Parameters	
PCBsats mass, m	0.1	kg
PCB area, A	9×9.5	cm^2
	Swarm parameters	
swarm population	10	-
$\sigma(\delta a_0)$	-58	m
$\sigma(a\delta\lambda_0)$	500	m
$\sigma(a\delta e_0)$	250	m
	Control parameters	
communication sphere radius, r_{bound}	200	m
safe along track shift	30	m
max drift threshold	100	m

- [6] D. Ivanov, U. Monakhova, A. Guerman, M. Ovchinnikov, and D. Roldugin, "Decentralized differential drag based control of nanosatellites swarm spatial distribution using magnetorquers," *Advances in Space Research*, vol. 67, no. 11, pp. 3489–3503, 2021. Satellite Constellations and Formation Flying.
- [7] S. Biktimirov, M. Akhloumadi, and D. Pritykin, "A femtosat swarm mission in leo: Differential drag control under power and communication constraints," *74th International Astronautical Congress*, 2023.
- [8] V. Beletsky and A. Yanshin, "Influence of aerodynamic forces on satellites attitude motion," 1984.
- [9] R. Wiltshire and W. Clohessy, "Terminal Guidance System for Satellite Rendezvous," *Journal of the Aerospace Sciences*, vol. 27, no. 9, pp. 653–658, 1960.
- [10] G. W. Hill, "Researches in the Lunar Theory," *American journal of Mathematics*, vol. 1, no. 1, pp. 5–26, 1878.
- [11] H. Schaub and J. Junkins, *Analytical Mechanics of Space Systems, Fourth Edition*. AIAA Education Series, 2018.